Static and dynamic testing of delamination in hybrid SHCC/concrete beams

Cabboi, Alessandro; Harrass, Othman ; Sánchez Gómez, Sergio; Lukovic, Mladena

DOI
10.1016/j.compstruct.2021.114961

Publication date
2021

Document Version
Final published version

Published in
Composite Structures

Citation (APA)
Cabboi, A., Harrass, O., Sánchez Gómez, S., & Lukovic, M. (2021). Static and dynamic testing of delamination in hybrid SHCC/concrete beams. *Composite Structures*, *281*, 1-14. Article 114961. https://doi.org/10.1016/j.compstruct.2021.114961

Composite Structures 281 (2022) 114961

Contents lists available at ScienceDirect

Composite Structures

journal homepage: www.elsevier.com/locate/compstruct

Static and dynamic testing of delamination in hybrid SHCC/concrete beams

Alessandro Cabboi *, Othman Harrass, Sergio Sánchez Gómez, Mladena Luković

Faculty of Civil Engineering and Geosciences, Delft University of Technology, Stevinweg 1, 2628CN, Delft, NL, Netherlands

ARTICLE INFO

Keywords:
Composite concrete beams
Strain Hardening Cementitious Composite
Experimental mechanics
Delamination
Structural health monitoring

ABSTRACT

The focus of this study is to characterize delamination using static and dynamic tests and to assess the interface failure mechanism of an innovative hybrid concrete beam, made out of conventional concrete and a special class of fibre reinforced material, known as Strain Hardening Cementitious Composite (SHCC).

Three SHCC beams were subject to four-point bending tests, differing in the interface surface preparation and curing method. Damage and delamination were gradually induced due to increasing loads in steps of 2.5 kN, and their propagation was tracked by the use of linear variable differential transformers and Digital Image Correlation technique. Dynamic hammer tests were also carried out to identify the natural frequency variation due to progressive damage. The outcome of this comparison allowed us to assess the capability of using a frequency-based monitoring technique for possible early-stage delamination detection of hybrid civil structures.

To understand the influence of delamination on the dynamic response, a simplified finite element modelling approach of delamination was adopted. The induced damage was modelled in a simplified manner by reducing the stiffness of the elements in the damaged area. This model can be potentially integrable into large-scale numerical models for Structural Health Monitoring purposes.

1. Introduction

The development of Structural Health Monitoring (SHM) strategies in Civil Engineering is usually driven by the concern of assessing the health condition of existing civil infrastructures [1–3]. Besides the challenge of assessing existing structures, SHM strategies become even more important for new structures built using novel materials, new structural systems and construction technologies, which are usually accompanied by a lack of experience on their application, lack of design codes and scarce knowledge on the long-term structural behaviour. Examples of new structural systems can be found in the domain of composite and hybrid structures [4–8], for which developing structural safety assessment techniques is of paramount importance due to the rudimentary knowledge of the interface mechanisms governing the debonding and fracture behaviour [9,10]. An innovative hybrid beam was recently proposed [11] by combining a conventional reinforced concrete beam with a special class of fibre reinforced ultra-ductile cement-based material, widely known as Strain Hardening Cementitious Composite (SHCC). The use of SHCC around the reinforcement in the tensile zone enabled controlled cracking behaviour with reduced crack widths, and could eventually lead to saving on reinforcement needed for crack width control in reinforced concrete structures. The governing factor that determines the performance of this hybrid concrete beam is the mechanical behaviour at the interface between the two concrete types [12]. The existence of a (non-reinforced concrete-to-concrete) interface in hybrid structures might trigger brittle failure, which could eventually be detected at an earlier stage by using proper monitoring techniques. Therefore developing monitoring strategies able to timely detect the initiation of a brittle failure is one of the biggest challenges within the SHM community.

Versatility is one of the main advantages of dynamic testing, since it can be either carried out in a laboratory environment or on real structures at a relatively low-cost and non-invasive way [13,14]. Therefore, dynamic testing, and the corresponding modal identification, is a commonly used technique also for assessing interface-related damage in composite structures [15]. Studies on vibration-based delamination detection are usually carried out in a controlled laboratory environment, and the success of the technique heavily depends on the amount of modal properties that can be identified from the dynamic tests. High order bending modes are usually more sensitive to local damage and relative changes between these identified modes allow the detection and localization of damage [16–19]. Further research efforts were devoted to improve the dynamic inverse problem aimed at detecting and localizing the damage by developing more robust optimization schemes, building upon physics-based models [20] or data-driven models [21]. Note that the majority of such type of studies, based on

* Corresponding author.
E-mail addresses: A.Cabboi@tudelft.nl (A. Cabboi), M.Lukovic@tudelft.nl (M. Luković).

https://doi.org/10.1016/j.compstruct.2021.114961
Received 12 June 2021; Received in revised form 24 September 2021; Accepted 3 November 2021
Available online 16 November 2021

modal tests and aimed at detecting delamination, are mainly restricted to layered laminates. Studies on delamination detection for reinforced concrete hybrid beams are still lacking.

In this study, three SHCC hybrid concrete beams, differing in the interface surface preparation and curing methods, were tested in four-point bending. The beams were made with a notch in the middle of the span in order to initiate the delamination. The initiation and propagation of the delamination between the concrete and SHCC layer were quantitatively tracked by the use of linear variable differential transformers (LVDTs). Digital Image Correlation (DIC) was used to track the deformations, strains and the crack development in the tested beams. Besides measuring the structural response related to static loading, hammer impulse tests were also carried out to assess the change of the dynamic response measured at different levels of damage by a set of accelerometers. This experimental investigation had two aims: to characterize the evolution of the damage mechanism during loading and the resulting failure mechanism by inspecting natural frequency shifts of the beams, load–displacement response curves and interface crack patterns detected by the DIC; and to evaluate the performance of dynamic testing, and corresponding modal identification, to detect interface-related damage for the proposed hybrid structure. This evaluation is supported by the measurements of the load deflection curves, accompanied by DIC and LVDTs placed along the interface since it is assumed that they would reasonably capture the damage, which could be linked with changes in natural frequencies. Note though, that such link may not hold for the general case, because internal damage is not captured by the DIC, and the crack pattern is neither simultaneous nor symmetric from both faces of the specimen due to the heterogeneous nature of concrete. The performance of the frequency-based damage detection technique was evaluated by identifying up to which extent, with reference to the remaining structural capacity of the beams, an interface-related damage of the hybrid beams can be detected.

As mentioned above, the success of a vibration-based delamination technique depends on the identifiability of higher bending modes. However, for large-scale civil structures, these higher bending modes (identifiable in a laboratory environment) are usually not excited or activated during actual operational and environmental conditions. Therefore, since the goal of evaluating the dynamic testing technique refers to its capability to be used for large-scale SHM campaigns, the current study limits the analysis to the fundamental frequency of the tested beams. In order to extract the most out of this analysis, two benchmark Finite Element Models (FEM) of the tested beams were developed. These models were used to simulate the observed damage-induced variation of the identified natural frequencies. The damage is modelled by reducing the Young's Modulus of selected elements in both FE models according to the delamination length and crack extension observed through the DIC results. The FE models and their updating strategy are kept simple, in order to allow a possible application within typical vibration-based SHM strategies relying on natural frequency variations [13,22–26]. In a very broad sense, a typical natural frequency-based SHM strategy includes a monitoring system that measures the dynamic response of the investigated structure under operational conditions and a data-processing methodology, which aims at translating the recorded data into valuable information for a safety structural assessment. To achieve the latter target, one approach consists in using Finite Element numerical models integrable with the measured data [13,22–26]. In order to apply this SHM approach on civil structures, detailed numerical models can become computationally expensive. Therefore, in order to speed-up the updating and calibration process, that usually relies on continuously recorded monitoring data (e.g. hourly data), the modelling of an hypothesized damage in the structure should be as simple as possible with the only constraint to properly mimic the effect that an eventual damage has on the modal properties. SHM guidelines on how to incorporate damage into large FE models in a simplistic manner are either not directly available or often proposed but not validated due to a lack of comparison with actual damage. Within this framework and with reference to the information retrieved from the FE models, this study also proposes simplified benchmark models (along the line shown in [23]) that allow to mimic the natural frequency shifts caused by the observed delamination and crack patterns, and that are able to be merged into an eventual vibration-based damage detection strategy, applicable on large-scale structures composed by means of hybrid structural elements.

2. Experiments and modelling

2.1. Experimental setup and methods

2.1.1. Experimental design

The hybrid reinforced concrete beams consists of two layers: the bottom layer, in which the reinforcement rebar is embedded, is made out of SHCC and the top one is formed by conventional concrete [11]. Since the behaviour of a hybrid structure is usually governed by the interface behaviour between the two materials, the test setup was designed in order to facilitate the investigation of the fracture behaviour of the structural interface (Fig. 1).

A conventional method to "directly" characterize the interface behaviour is the so called bond test [27–29]. However, in this study, a four point bending test setup was designed to characterize the interface behaviour of the hybrid beams. In order to generate stress concentrations close to the interface, the SHCC layer of the hybrid beam was split in two parts by inserting a joint in the middle (see Fig. 1). In such regard, extensive studies on testing the interface between precast floor planks and the in-situ cast concrete [30,31] prove that the investigated setup and loading conditions are critical for the interface behaviour. Due to the middle joint and the specific steel reinforcement arrangement (see Fig. 2), there is a high probability that the interface failure between SHCC (labelled in yellow) and conventional concrete (labelled in grey) will occur. Monolithic, composite action at the connection between the two prefabricated SHCC elements, is enabled by the bond between SHCC and concrete. This bond enables the stress transfer from the rebars, embedded in the SHCC layers, to the reinforcement bars placed at the bottom part of the concrete layer, referred to as coupling flexural reinforcement. The length of this coupling reinforcement is 600 mm. However, no vertical reinforcement (e.g. stirrups) are crossing this coupling reinforcement, therefore the efficiency of the calculated transfer length is not optimal.

In order to monitor the interface fracture behaviour and the global dynamic response of the beams, an extensive monitoring system was installed. LVDTs were mounted along the interface from one side of the beams and DIC was carried out from the opposite side of the beams. Accelerometers (labelled with red dots, see Fig. 2) were placed at the top and at the bottom of the beams, as well as LVDTs along the joint, installed at the bottom of the beams.

2.1.2. Specimen preparation and casting

Both the concrete and the SHCC layer were reinforced with longitudinal and vertical steel bars (see Fig. 2). First, the SHCC layer with a thickness of 70 mm was cast. A plastic spacer was placed in the middle in order to generate the aforementioned joint, separating the layer in two parts. After casting of the SHCC layer, the specimens were compacted at the vibration table for 30 s. Longitudinal reinforcement was embedded in these SHCC layers, whereas vertical stirrups were sticking out. The stirrups were placed outside the constant moment region. After 2 days of sealed curing of SHCC, the coupling reinforcement is placed and ordinary concrete was cast on top of the precasted SHCC layer.

The SHCC and concrete mix composition are summarized in Table 1. They are the same as the one used in the previous study [11]. Prior to concrete casting, the interface (i.e. the top surface of SHCC) was cleaned with air jet, subsequently wiped by a steel brush, and finally cleaned with ethanol in order to remove surface dust and provide a good bond. Three types of samples were prepared. In two samples,

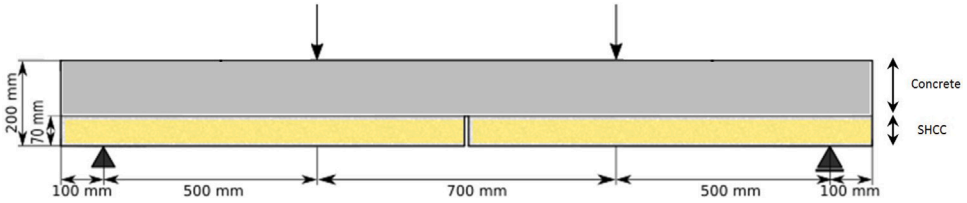

Fig. 1. Test set-up for investigating the interface behaviour in the SHCC hybrid concrete beam.

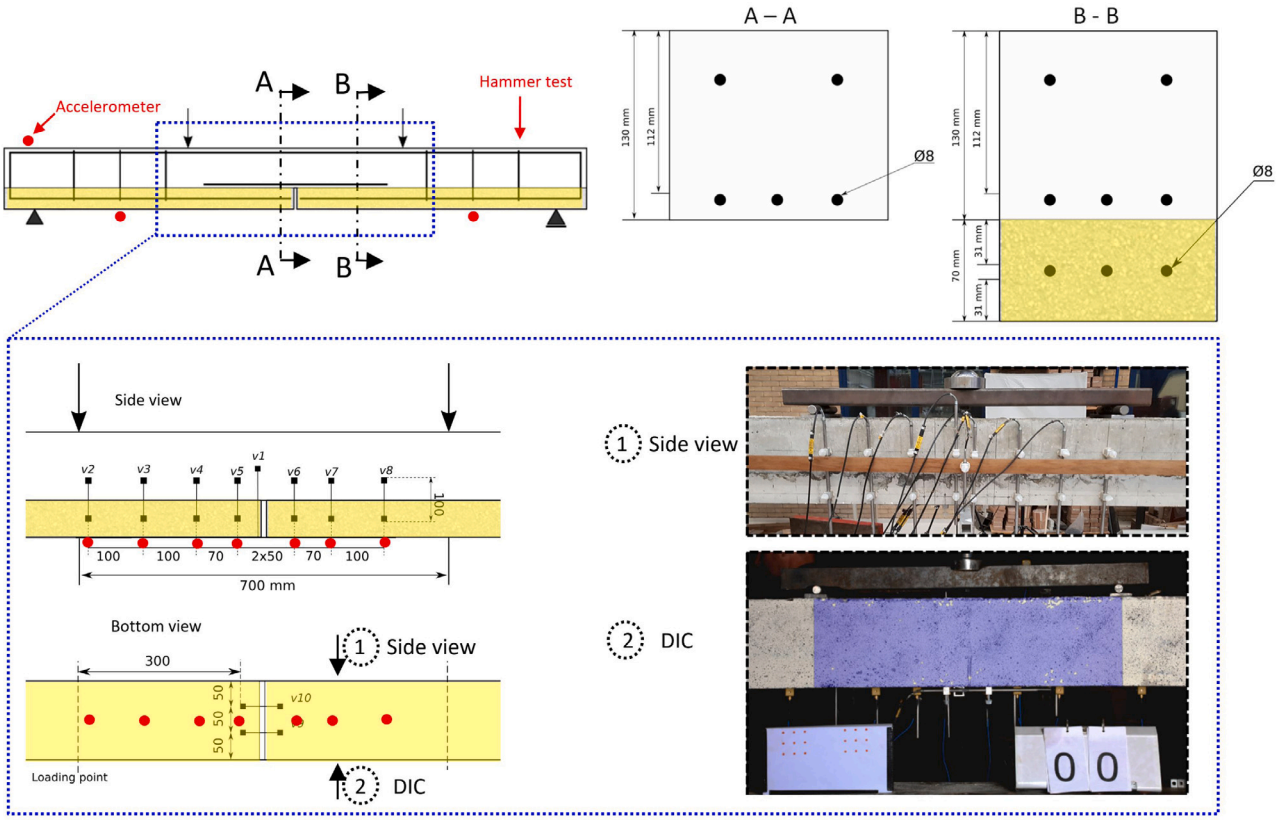

Fig. 2. Experimental setup with reinforcement design and distribution of measuring devices: accelerometers, LVDTs (labelled with v) and DIC. (For interpretation of the references to colour in this figure legend, the reader is referred to the web version of this article.)

Table 1
SHCC and concrete mixture composition.

Material (amounts in [kg/m^3])	SHCC	Concrete
CEM III B	790	–
CEM I 52.5 R	–	260
Limestone powder	790	–
Sand (0.125–4 mm)	–	847
Gravel (4–16 mm)	–	1123
PVA fibres	26	–
Water	410	156
Superplasticizer	2.13	0.26

concrete was directly added on top of the prepared smooth interface, while in the third sample, an epoxy layer was added on the interface in order enhance the bonding strength with the concrete. Subsequently, sand with varying size (1–2 mm) was sprayed on top of the epoxy layer (see Fig. 3). This sample is labelled as "Epoxy" sample.

In order to investigate the effects of the curing method on the interface behaviour, one of the two samples with the smooth interface (labelled as "Curing") was taken out of the mould after 7 days of sealed curing and exposed to drying conditions in a humidity-controlled (50%) room. After 4 weeks of drying, this sample was ready for the four point bending tests. The remaining two specimens ("Reference" and "Epoxy") were taken out of the mould after 33 days of sealed curing and also prepared for the mechanical tests.

In addition to the cast beams, standard cubes (150 × 150 × 150 m^3) were cast to determine the compressive strength of the components. The average compressive strengths of concrete and SHCC at the age of testing were 50 MPa. The elastic modulus and density of SHCC were retrieved from an earlier study [32], whereas the elastic modulus and the density of the conventional concrete are determined based on its measured compressive strength, using the well established analytical expressions provided by the Eurocode [33].

2.1.3. Testing

The tested beams were loaded step-wisely in steps of 2.5 kN until ultimate failure occurred. After each loading step, specimens were unloaded and hammer tests were carried out. The dynamic responses were recorded at several locations on the bottom part of the tested beams as shown in Fig. 2. The dynamic test setup consists of 10 tri-axial ceramic shear ICP accelerometers (model type 356B18) and an instrumented ICP impact hammer with a soft plastic tip (model type 086D50). Each accelerometer has a sensitivity of 1 V/g and a linear frequency response

Fig. 3. Different types of interface preparation: smooth ("Reference" and "Curing") and "Epoxy" sample with sand at the surface.

between 0.5–3000 Hz. The dynamic responses were recorded with a frequency sampling of 25 600 Hz (the sampling rate was a fixed one given by the data acquisition device) and each measurement had a duration of 5 s. The dynamic impulses were applied on top of the beam, at the location indicated in Fig. 2, and the corresponding frequency response functions (FRFs) were estimated after applying a low-pass filter with a cut-off frequency of 1500 Hz and decimating the time-series by a factor of 10. The FRFs were then computed based on the H_1 estimator [34] and averaging over three impacts and their corresponding free decay dynamic responses. A linearity check of each FRF was also performed by inspecting its corresponding coherence function. Once all the FRFs were estimated, the inverse Fourier transform was applied in order to retrieve the representative impulse response functions (IRF) which have a reduced level of noise compared to the original free decays. Natural frequencies and mode shapes are then identified by applying an automated version of the Eigensystem Realization Algorithm (ERA), see [35], on the estimated IRFs.

During the tests, the DIC technique was used to evaluate the crack pattern development and crack widths [36] at each loading step (see Fig. 2). The DIC is a non-contact optical method that employs tracking and image registration techniques for accurate 2D measurements of changes in images, which allows to calculate deformations, displacements and strains on the observed surface. The technique became widely used in the concrete scientific community [37]. Besides the DIC measurements, as already pointed out, LVDTs were used for verification and to accurately measure the vertical displacements of the beams and the resulting interface and joint openings.

2.2. Finite element model

In order to facilitate the interpretation of the hammer test results, two FE models were developed with ABAQUS 6.14 [38]. The first FE model (model 1) is merely used to check possible dynamic interactions between the supporting steel beam and the hybrid concrete beam (see Fig. 4). Therefore, model 1 covers the whole test setup, including both the hybrid concrete beam and the supporting steel beam. The supporting steel structure is an I-shape profile beam, 3.5 m long. The steel beam is assumed to be clamped at both ends. For the purpose of carrying out a modal analysis, the connection between the steel beam and the hybrid concrete beam is modelled by assuming an ideal bond along a line contact between two supporting rollers and the tested beams. The second FE model (model 2) simulates the tested hybrid beams only, which is assumed to be simply supported. As later explained, model 2 was used as a reference model, to mimic the effects induced by the occurrence of damage on the identified modal properties of the hybrid beams.

A linear elastic constitutive law is used for both concrete and SHCC with Young's Modulus E of 35 GPa and 22 GPa, and material density ρ of 2400 kg/m^3 and 2000 kg/m^3, respectively [32,33]. The Poisson coefficient for both layers is assumed to be 0.2. The middle joint was simply taken into account by removing a vertical stripe with a thickness of 10 mm. In addition to the aforementioned material layers, the steel reinforcement of the specimens was also included in both FE models, represented by longitudinal steel bars and vertical stirrups with a Young's Modulus of 200 GPa and a density of 7850 kg/m^3. Note that the beams are designed such that the steel behaves in an elastic way, therefore its inelastic properties are not relevant for the presented study. The elastic modulus and density of steel are provided by the steel producer and are not expected to show large variability. The interaction between the two concrete layers, and between the steel bars and the concrete layers were modelled by assuming an ideal bond, neglecting eventual slip mechanisms. Since the main focus in Section 4 is on FE model 2, the adopted mesh of such model consists of 3D 60 270 linear hexahedral elements and 1482 linear line elements, with a total of 69 317 nodes.

In order to mimic the damage-induced frequency variations and for a comparative purpose, two submodels of model 2 were developed. The first submodel (model 2.1), makes use of a small fixed damaged volume ($80 \times 150 \times 40$ mm^3) confined in the centre of the beam. The Young's Modulus of such volume was taken as an updating parameter in order to match the observed frequency variation. The aim of the FE submodel 2.1, as will be shown in Sections 3 and 4, is mainly to capture the

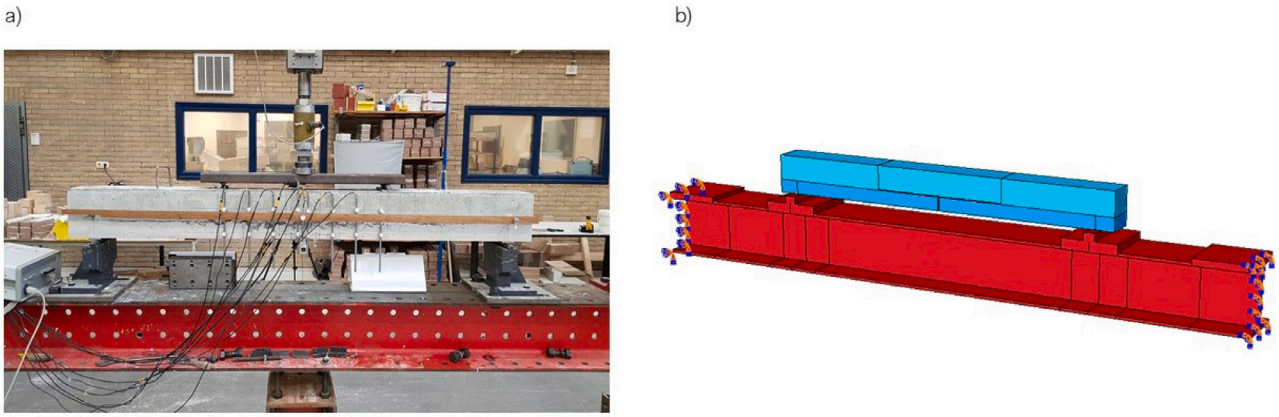

Fig. 4. Experimental setup: (a) photo taken in the laboratory of the tested hybrid beam and supporting steel beam; (b) snapshot of FE model 1.

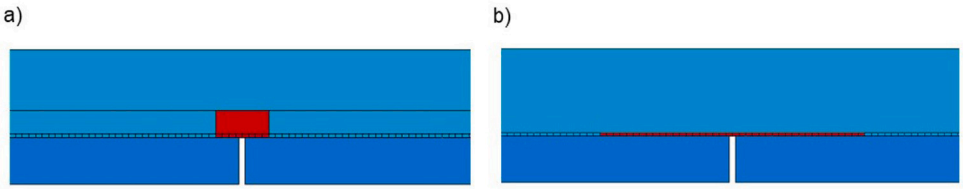

Fig. 5. Assumed damaged zone (red area): (a) FE model 2.1; (b) FE model 2.2. (For interpretation of the references to colour in this figure legend, the reader is referred to the web version of this article.)

damage observed for the Epoxy beam. The second submodel (model 2.2), assumes the presence of a horizontal elastic "debonding" sheet between the concrete layer and the SHCC layer, with a height of 5 mm and a length of 700 mm. The "debonding" layer is split into segments of 10 mm length having the same height and covering the beam width. Again, the Young's Modulus of the debonding layer is assumed as an updating parameter. The aim of the FE submodel 2.2 consists in capturing the damage observed for the Reference and the Curing beam. For both submodels, the starting reference mechanical properties of the damages zone are assumed to be equal to the concrete material.

3. Experimental results

3.1. Fracture behaviour of the beams

The DIC results enable to visualize the crack propagation resulting from increasing loading steps. For such purpose, a validated method consisting of estimating the equivalent von Mises strain [39] from the DIC measurements was used. Although von Mises strain is usually used to evaluate the occurrence of yielding in ductile materials, a high concentration of such strains is strongly linked to crack formation and as such, von Mises strains are commonly used in combination with DIC to clearly visualize cracks in concrete and masonry structures [39,40]. First, the experimental results for the Reference sample will be discussed and, subsequently, the behaviour of the samples prepared with a different curing method and interface roughness (Curing and Epoxy sample, respectively) will be compared to the Reference one.

Fig. 6 refers to the Reference sample and provides an overview of the applied load levels, the corresponding measured vertical displacements, the joint and interface openings and the damage pattern revealed by the DIC. The measured vertical displacements refers to sensor v1, while the interface and joint openings refer to the maximum values obtained between the sensor pairs v5–v6 and v9–v10 (see Fig. 2). The DIC snapshots are linked to the legend, indicating the von Mises strains. Note that this legend is kept constant throughout the whole paper. The surface contours shown in the DIC snapshots refer to the constant bending moment region defined by the blue-marked region in Fig. 2. It can be observed that the damage starts with a vertical crack localized at the location of the notch. Successively, delamination develops along the interface. Although delamination is the governing failure mechanism, the DIC results reveal that the sample exhibits also a combination of delamination and vertical, flexural cracking. This is especially visible for applied loads higher than 10 kN. The ultimate failure occurs due to delamination of the interface and rupture of the beam at the end of the coupling reinforcements, at a load level of approximately 14 kN, see also Fig. 7.

In Fig. 8 the results for the Reference and the Curing beam are compared. In both load–displacement curves (Fig. 8a), the red circles indicate the points for which the DIC snapshots of the crack history are provided. In order to enable a better comparison between the two samples, at the same loading level, the length of delamination was also measured and indicated in the DIC snapshots of Fig. 8. The slope difference of the load–displacement curves in Fig. 8a shows that the stiffness of the Curing sample subjected to a shorter curing process is lower compared to the Reference sample. This might be due to shrinkage, also given the fact that some shrinkage induced cracks were observed at the surface of the SHCC layer in the Curing sample before applying the mechanical loading. Note that no additional shrinkage measurements were performed for these beams, so no further evidence is available to support the aforementioned hypothesis. Still, given that the shrinkage strain for this SHCC mix is significantly larger than that of conventional concrete [41], and that the only difference between the samples is the different curing procedure, it could be assumed that the restrained shrinkage might have had a large influence. This will be a subject of future studies. The DIC results also reveal that the Curing sample is characterized by a somewhat larger delamination length at the same applied load, exhibiting less flexural cracks compared to the Reference sample. Despite these differences in stiffness and damage propagation, the joint and interfaces openings measured for the Reference and Curing beams are fairly similar, as shown in Fig. 8b. In addition, despite the slope differences shown in Fig. 8, the type of failure and the measured ultimate load for both beams are almost identical, meaning that the different curing conditions did not alter the structural capacity of the two beams.

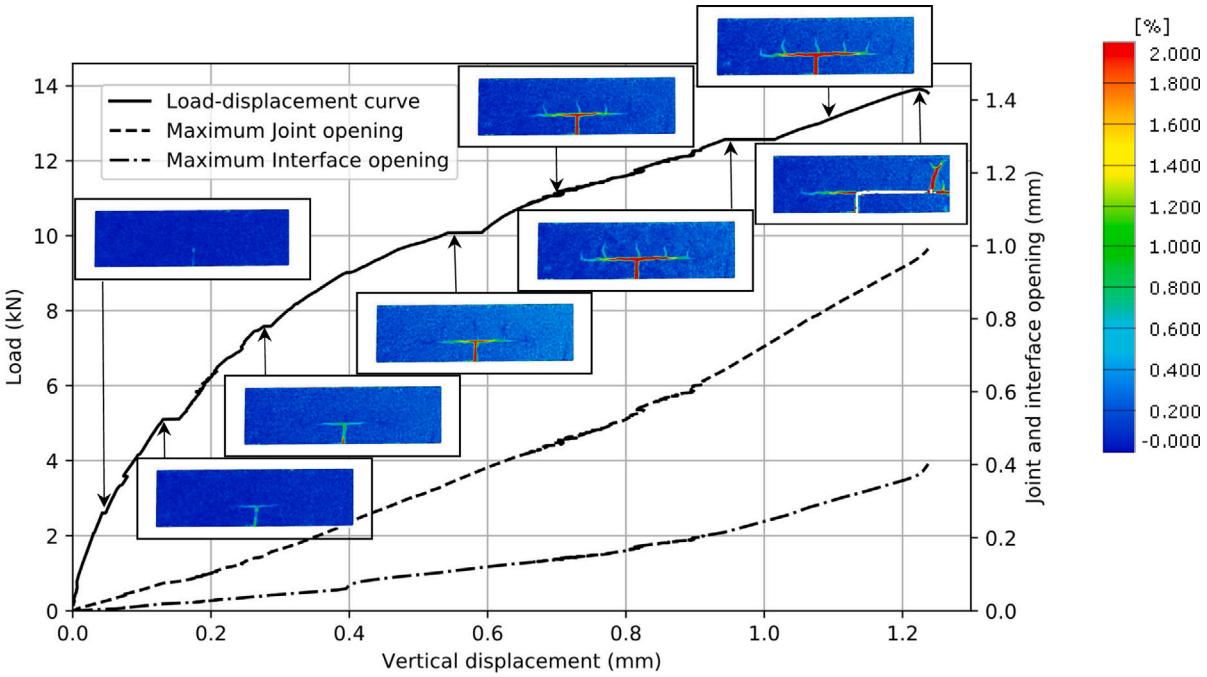

Fig. 6. Reference sample: load vs. displacement and load vs. joint and interface opening, with corresponding damage propagation obtained by the DIC. The legend on the right side indicates the equivalent von Mises strains. Note that the same legend is used in all the DIC graphs.

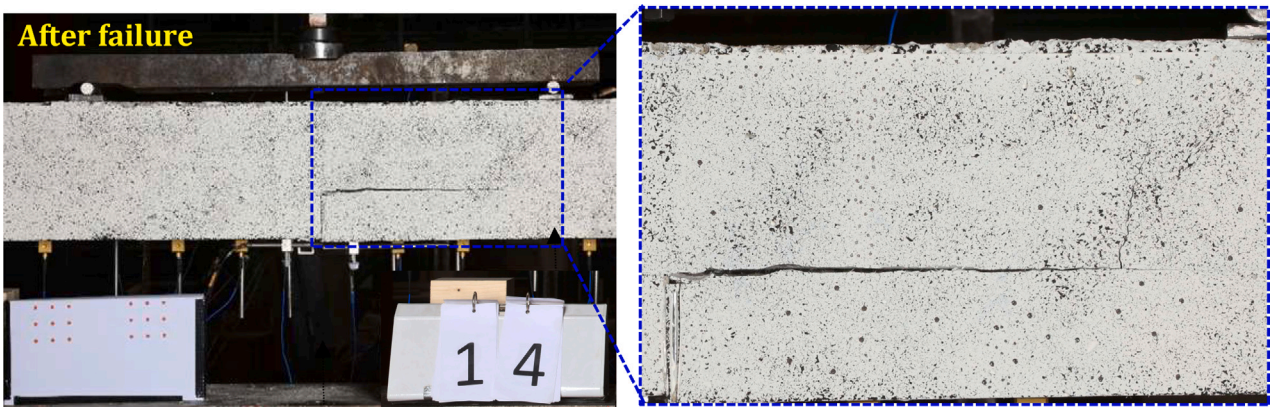

Fig. 7. Final failure in the Reference sample.

The load–displacement curves and the load versus maximum joint and interface opening, with corresponding damage propagation for the Reference and the Epoxy sample, are shown in Fig. 9. It can be observed that, unlike for the Curing sample, the slope of the load–displacement curves of the two beams almost overlap, indicating a similar bending stiffness. However, the results indicate a significant difference in the fracture behaviour and in the structural capacity of the beams. The structural capacity of the Epoxy beam is more than 50% higher than that of the Reference and Curing sample. This can be explained by a fundamentally different failure mechanisms occurring in the Epoxy sample. Whereas in the Reference and the Curing beam the damage was triggered and driven by delamination, in the Epoxy sample a vertical flexural crack originated from the middle vertical notch, dominating the damage mechanism until a loading level of 10 kN was achieved. Subsequently, more flexural cracks, combined with limited and localized delamination occurred.

Based on the presented results, for the Reference and Curing sample the main failure mechanism appeared to be delamination, while for the Epoxy sample flexural cracking seems to be the governing failure mechanism. Note that the maximum joint and interface opening at the same load level is also significantly reduced in the sample with epoxy surface, as illustrated in Fig. 9b. As a final note, the crack pattern of the collapsed Epoxy sample kinked in the concrete layer (see Fig. 10). In order to better understand and characterize the propagation of this crack, after the test, the Epoxy beam was cut in the middle along its longitudinal axis. It was observed that the crack propagated along the interface only shortly in the vicinity of the notch, subsequently kinking to the horizontal coupling reinforcement in the concrete layer (see Fig. 11). The failure occurred due to the propagation of this crack along the coupling rebar. Therefore, the test on the Epoxy sample only partially provides meaningful insights into the fracture behaviour of the interface itself.

3.2. Frequency response function and comparison with FE model

Fig. 12 shows the estimated frequency response functions (FRFs) from the dynamic responses recorded at location v6 (bottom side of the beam) for the Reference beam. Each FRF is estimated based on three dynamic responses triggered by hammer hits applied on top of the beam along the vertical direction (see Fig. 2). An example of a stabilization

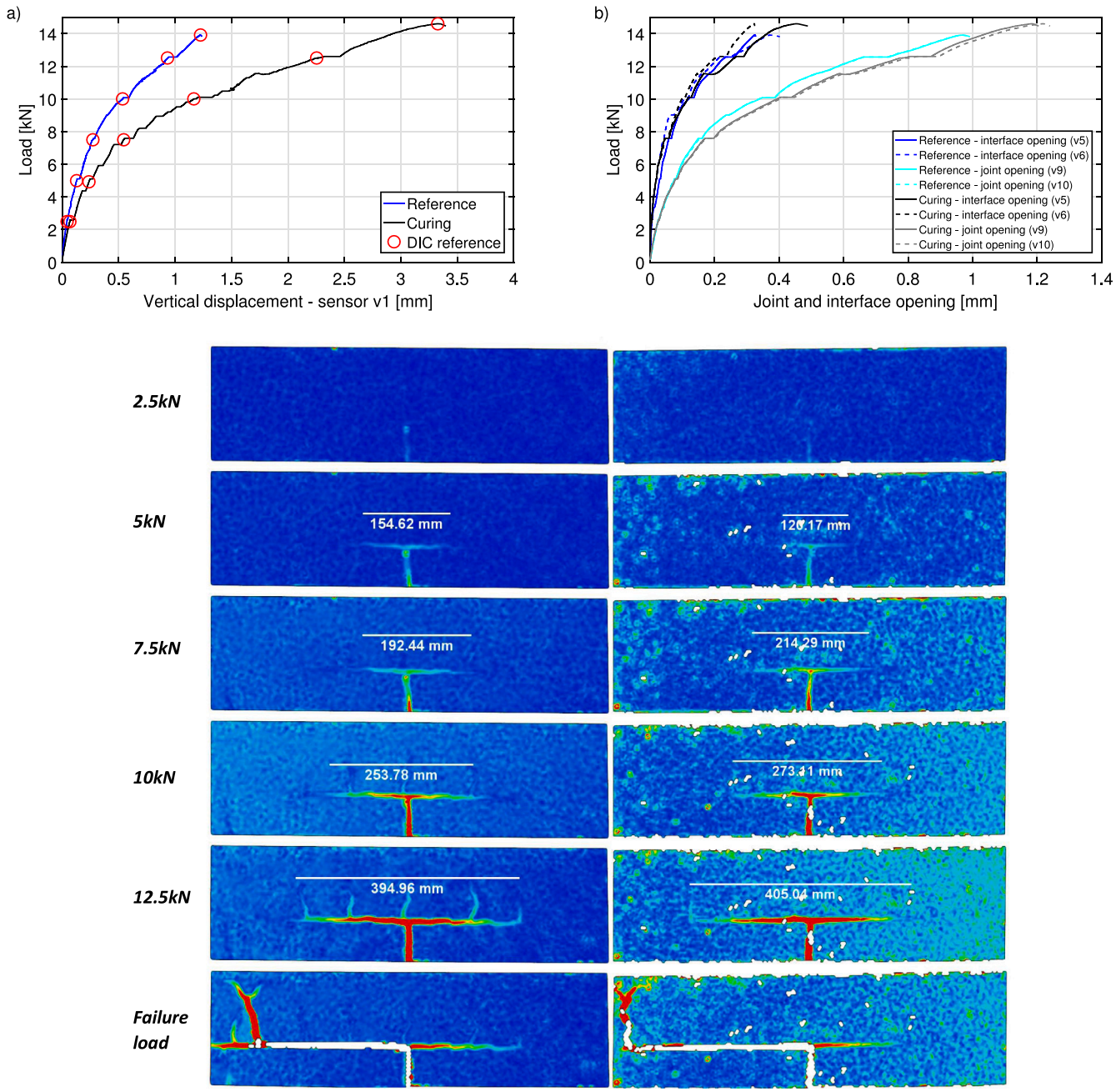

Fig. 8. Reference and Curing sample: (a) applied load vs. vertical displacement measured at sensor v1; (b) applied load vs. joint and interface opening. The figure below, shows the damage propagation in the Reference (left) and the Curing (right) beam for increasing loading steps corresponding to the red circles in (a). The same Von Mises strain legend as given in Fig. 6 is used.

diagram, overlapped with one FRF to facilitate the interpretation, is shown in Fig. 12a, visualizing the identified system poles (vertically aligned black dots) for different model orders obtained through the ERA technique. Fig. 12b contains 7 FRFs referring to the dynamic responses of the same location, estimated before and in between the increasing loading steps. The effect due to the progressive damage is clearly visible through a step-wise decrease of the natural frequencies. Below 100 Hz and along the vertical direction, two frequency peaks are detectable. The first one around 47 Hz and the second one around 94 Hz. By carrying out a modal analysis of FE model 1, which simulates the whole test setup, an estimate of the mode shape corresponding to the first observed frequency peak is provided (see Fig. 13a). The identified mode shape is mainly driven by the top flange motion of the bottom steel beam. The second identified frequency peak is linked to the first bending mode of the tested hybrid beam. FE model 2 estimated the first bending mode at 92.38 Hz, which corresponding mode shape is illustrated in Fig. 13b. A similar bending mode around 90 Hz was also observed in FE model 1. In general, a fairly good comparison between the numerically estimated and experimentally identified bending mode shapes is highlighted in Fig. 14a. Among the few identified modes along the vertical direction (in few occasions the second bending mode was identifiable), the first bending mode of the hybrid beam turned out to be the most reliable one to capture the influence of the damage induced on the tested beams.

Fig. 14b shows the decreasing trend of the normalized natural frequency of the first bending mode of the three tested beams. The decrease is correlated to the progressive applied load. The similarities and differences in the structural capacity between the three beams

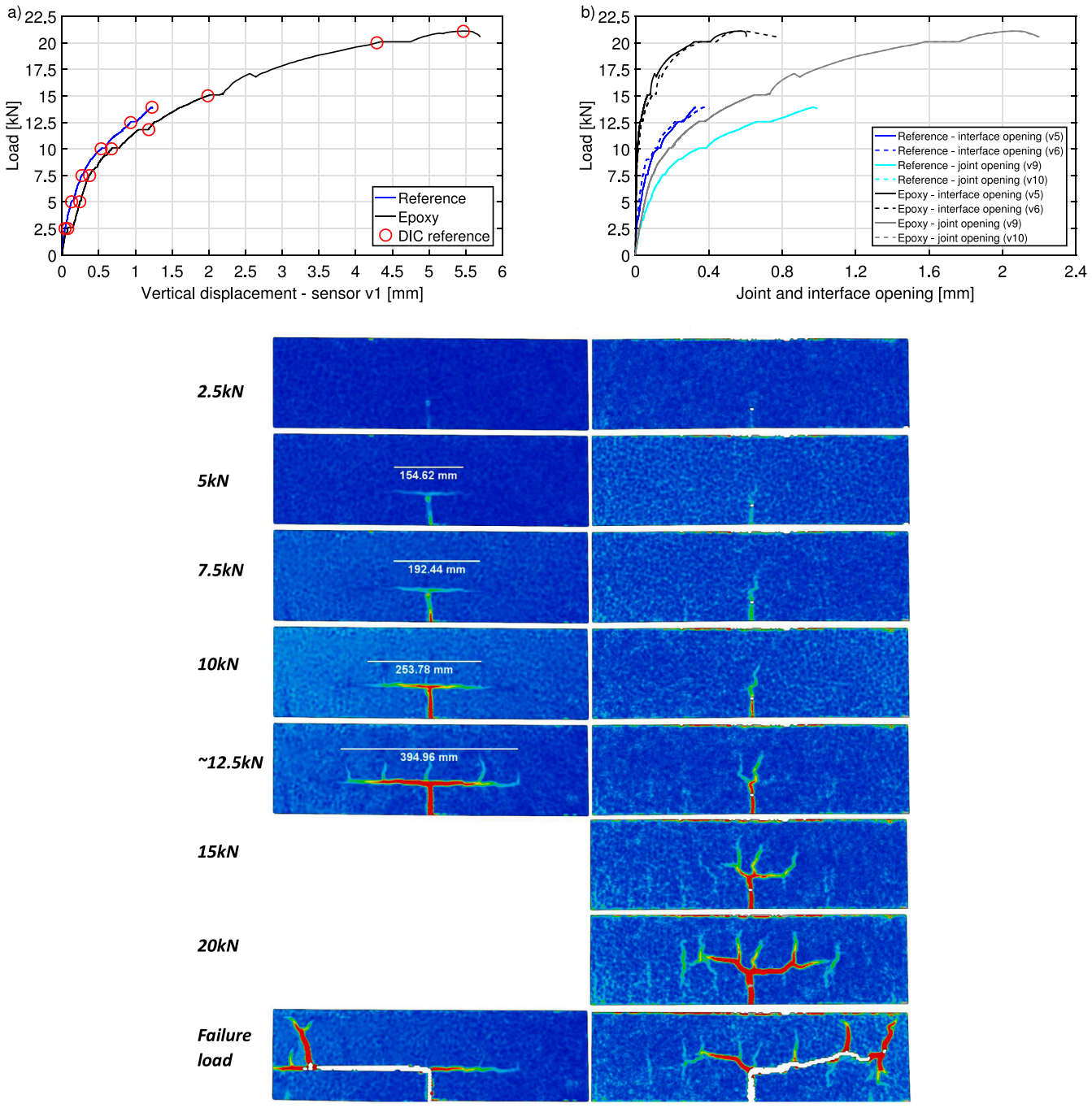

Fig. 9. Reference and Epoxy sample: (a) applied load vs. vertical displacement measured at sensor v1; (b) applied load vs. joint and interface opening. The figure below, shows the damage propagation in the Reference (left) and the Curing (right) beam for increasing loading steps corresponding to the red circles in (a). The same Von Mises strain legend as given in Fig. 6 is used.

observed in Section 3.1 are also reflected in Fig. 14b. The Curing and Reference samples exhibit a comparable behaviour in terms of decrease of the natural frequency. On the other hand, the slope of the curve showing the natural frequency decrease is slightly lower for the Epoxy sample, which exhibited a higher structural capacity (Fig. 9). Interestingly, all three beams exhibited a 10% frequency reduction just one load step before failure (i.e. at a load level which is approximately 15% lower than the failure load).

4. Simulated delamination-induced frequency shifts

The target of the developed submodels, FE model 2.1 and 2.2, is not to simulate the physics of the crack propagation, for which more advanced models would be necessary [42], but to use a simplified approach able to reproduce the observed damage-induced effects on the fundamental natural frequency of the hybrid beams. The advantage of mimicking the observed effect through a simplified approach, is that it can be easily implemented in larger and more detailed FE models representing full-scale structures, enabling such models to support frequency-based damage detection strategies in real-time, if needed. As mentioned above, the tuning parameter used to simulate the natural frequency variation caused by the observed delamination and crack phenomenon is the Young's Modulus of the assumed damaged zone in FE model 2.1 (Fig. 5a) and of the debonding zone in FE model 2.2 (Fig. 5b).

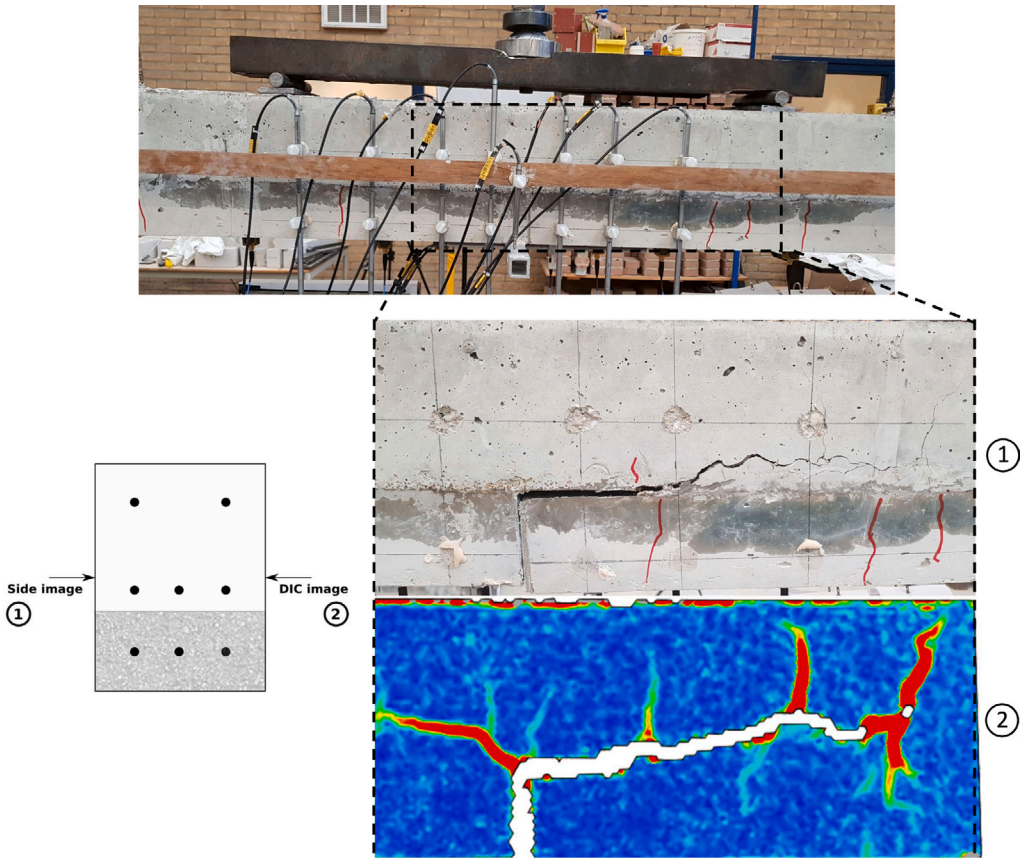

Fig. 10. Final damage in the Epoxy sample, both from the side where the DIC and LVDTs were placed. Note that, as earlier explained, the damage is not symmetrical from both sides of the beams.

Fig. 11. Crack propagation in the Epoxy sample, within the beam, observed after cutting the sample in the middle.

4.1. FE model 2.1

FE model 2.1 assumes a damaged area at the centre of the beam, as shown in Fig. 5a. This centred damaged area was approximately defined based on the significant strain concentrations that were observed in all samples within that area, especially with reference to the Epoxy sample. The size of the damaged area remained fixed, while the corresponding Young's Modulus was step-wisely reduced from 35 GPa to 35 MPa at each modal analysis run. Each reduced Young's Modulus value was kept constant throughout the modelled damaged area. The outcome of such step-wise reduction of the Young's Modulus allowed to estimate the required elastic modulus reduction of the damaged area in order to match the experimentally observed shifts of the natural frequencies. Therefore, the grey continuous line in Fig. 15a represents the simulated trend of the natural frequency reduction corresponding to the first bending mode with decreasing values of the Young's Modulus. Experimentally observed frequency reductions for the three tested beams were used to intersect the simulated curve of natural frequency reduction in order to identify the corresponding decrease of the Young's Modulus for different levels of damage. It can be observed that for a 5% natural frequency reduction, a relatively high Young's Modulus reduction is required (more than 60%). Furthermore, a 50% reduction of the Young's modulus corresponds to a natural frequency reduction of merely 2.5%. Note that this marginal frequency reduction falls within the observed standard deviation of identified natural frequencies from ambient vibration monitoring campaigns [43–46]. Finally, as observed in Fig. 14b, the maximum frequency reduction just before the failure is merely 10%, corresponding to a Young's Modulus reduction of around 80%.

4.2. FE model 2.2

FE model 2.2 is a more representative model of the delamination process since it also includes the information about the experimentally observed debonded length. This model was used to mimic the frequency shifts of the Reference and the Curing sample, since the delamination in the Epoxy sample was limited. Fig. 15b shows a 3D surface of the estimated natural frequency reduction for a given Young's Modulus reduction, considering the actual, i.e. experimentally measured, delamination length. Therefore, for a fixed delamination length, different values of Young's Modulus were ascribed (from 35 GPa down to 35 MPa) and the corresponding natural frequency reduction was evaluated. The delamination length varied between 0 and 700 mm with a step-wise increase of 20 mm. In each simulation, the reduced value of the Young's Modulus was assumed constant throughout the chosen delamination length. The 3D surface shown in Fig. 15b, was

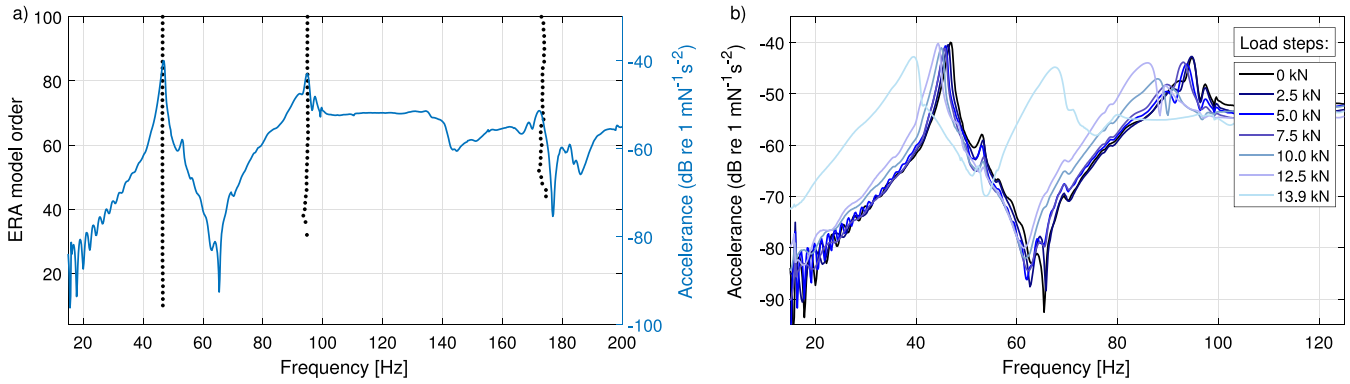

Fig. 12. (a) Identified system poles by means of the ERA method for different model orders and estimated FRF for the Reference beam; (b) estimated FRFs before and after each loading step up to failure (13.9 kN) for the Reference beam.

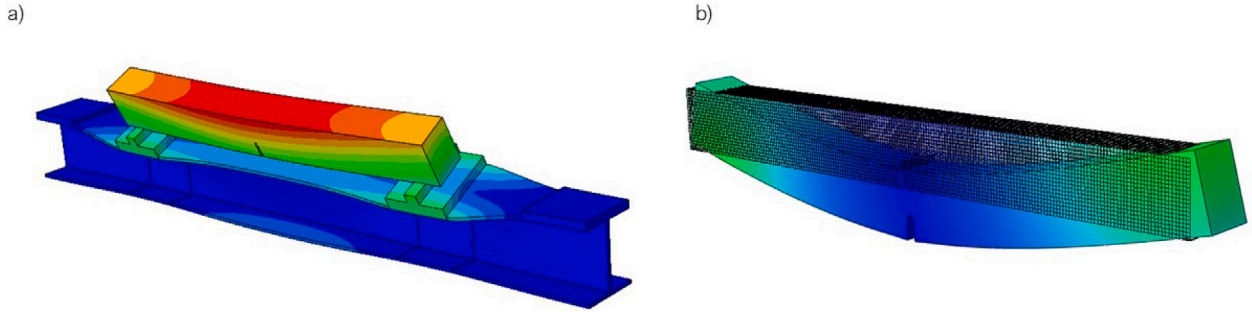

Fig. 13. (a) Simulated mode shape at 45.83 Hz (FE model 1); (b) simulated bending mode shape of the tested hybrid beam at 92.38 Hz (FE model 2).

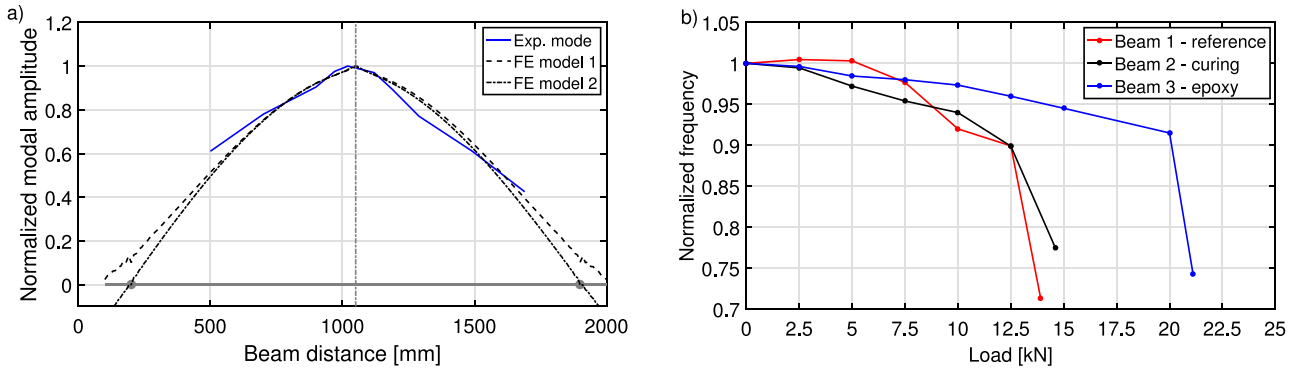

Fig. 14. (a) Comparison of the first bending mode shape between FEM and experimental result; (b) decrease of normalized frequency vs. applied load during static tests.

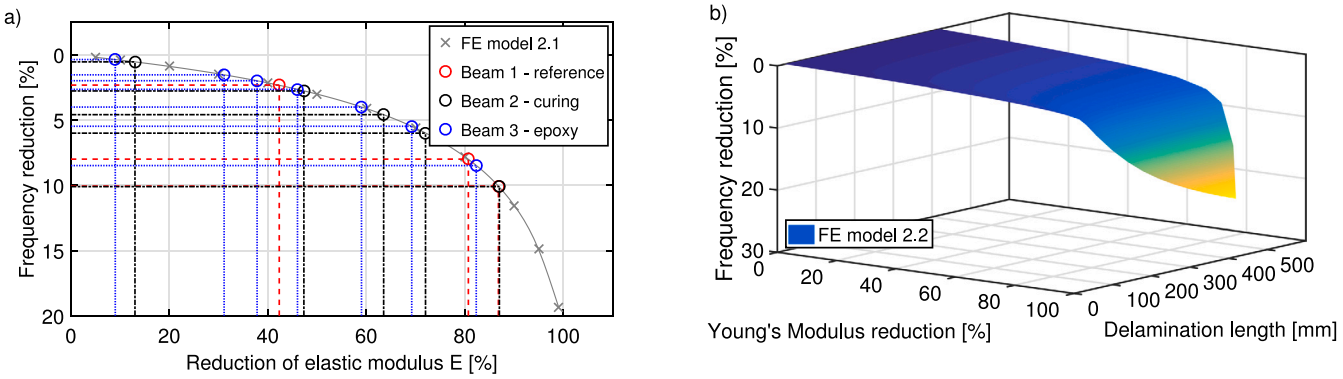

Fig. 15. (a) Delamination-induced frequency shifts simulated by submodel 2.1 due to a reduction of the Young's Modulus and measured frequency variation of the first bending mode for all three beam samples; (b) delamination-induced frequency shifts simulated by submodel 2.2 due to a reduction of the Young's Modulus and an increase of the delamination length.

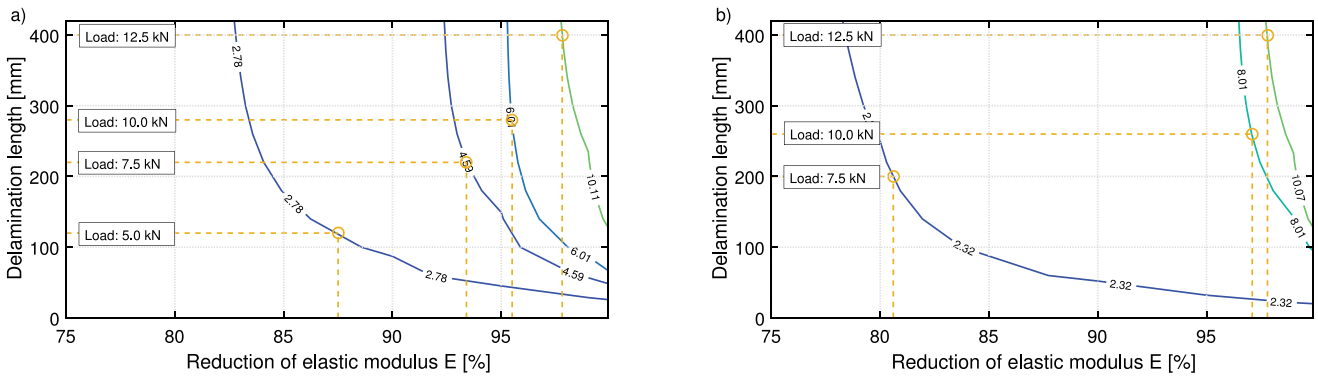

Fig. 16. Contour lines of the simulated delamination-induced frequency shifts and corresponding elastic modulus reduction for (a) Curing and (b) Reference sample.

Table 2
Summary of the identified experimental frequencies, measured delamination lengths and estimated Young's Modulus. For the Epoxy sample, the estimated Young's Modulus only refers to FE model 2.1, while for the Reference and Curing samples, the values for both FE models (2.1/2.2) are reported.

Loads [kN]	Delamination [mm] (exp)		Frequency [Hz] (exp)			Young's Modulus [GPa] (FE)		
	Reference	Curing	Reference	Curing	Epoxy	Reference FE 2.1/2.2	Curing FE 2.1/2.2	Epoxy FE 2.1
0	–	–	93.5	92.8	90.0	35/35	35/35	35
2.5	–	–	93.9	92.3	89.7	–	30.5/–	31.9
5.0	155	125	93.8	90.3	88.6	–	18.4/4.4	24.1
7.5	192	214	91.2	88.6	88.2	20.2/6.8	12.8/2.3	21.8
10.0	254	273	86.0	87.3	87.6	6.8/1.0	9.8/1.6	18.9
12.5	395	405	84.1	83.5	86.4	4.6/0.8	4.6/0.8	14.4
15.0	–	–	–	–	85.1	–	–	10.8
20.0	–	–	–	–	82.1	–	–	6.2

then used with reference to the observed delamination length for the Reference and Curing beam. The contour lines in Fig. 16a and Fig. 16b correspond to the observed natural frequency reduction expressed in percentage (see text within the contour lines) of the Reference and Curing sample. The measured delamination lengths taken from both beams (see Fig. 8) were then used to intersect (see yellow dashed lines) the selected contour lines in order to pin down the corresponding Young's Modulus reduction of the thin elastic layer representing the debonding zone.

Unlike the Young's Modulus reduction estimated from model 2.1 (which were in range up to 80%), with a more precise damage representation, the required Young's Modulus reduction needed to match the different identified bending mode frequencies of the beams turned out to be larger than 80%. Note that the latter observation is linked to the assumed and fixed height of the simulated debonded layer. Specifically, for a Young's Modulus reduction between 0 and 80%, the influence of the delamination length on the natural frequency variation of the first bending mode is negligible. Whereas within the range of 80% and 99% of the Young's Modulus reduction, the delamination length between 0 and approximately 200 mm significantly affects the natural frequency of the first bending mode. In comparison to FE model 2.1, in order to achieve a natural frequency reduction of 2.5%, a Young's Modulus reduction of 90% would be needed for a delamination length of 80 mm (the length of the assumed damage zone in FE model 2.1). Therefore, a more "realistic" representation of the delamination zone would inevitably require a larger elastic modulus reduction to match the experimentally observed natural frequency shifts.

Table 2 provides a summary of all the identified frequencies and corresponding Young's Modulus needed for FE model 2.1 and 2.2, and the measured delamination length for the Reference and Curing sample.

5. Discussion and recommendations for frequency-based damage detection

In order to facilitate the comparison between the results shown in Sections 3.1 and 3.2, Fig. 17 overlaps the identified natural frequency decrease of all the beams with the measured vertical displacements (Fig. 17a) and the averaged interface opening between sensor v5 and v6 (Fig. 17b). The difference of the structural capacity between the Epoxy sample and the Reference and Curing sample can be detected in both the static- and dynamic-related properties. However, no further similarities between the two type of information can be deduced. Overall, the load–displacement curves and the DIC results provide more valuable insights with reference to the characterization of the delamination process and the structural capacity of the beams than the information retrieved by the hammer tests. The load–displacement curves, for example, exhibit a neat slope difference (after a load of 5 kN) between the Curing and the Reference (or Epoxy) beam, while the slope of the natural frequency–load curve is less clear and more scattered. This scatteredness is mainly due to the non ideal testing setup for the dynamic measurements. The hammer tests were carried out after each loading step with the beam supported by two rollers. In order to avoid excessive movements of the beam and of the rollers, which could have caused a misalignment for the static test, the hammer hits were rather gentle, inducing a moderate excitation of the beam. In addition, the location of the hammer hits was close to one of the roller supports, which is not ideal to trigger a proper dynamic response for dynamic identification purposes. The consequences of these non ideal conditions are reflected by the FRFs shown in Fig. 12, in which only the first bending mode (in addition to the steel flange mode) of the tested beam was detectable. The second bending modes of the beams were detectable only in very few occasions and were therefore neglected for this study.

A final analysis was carried out by inspecting the correlation between the decrease of the normalized natural frequencies and the remaining structural capacity of the beams, shown in Fig. 18. The remaining capacity is expressed in percentage, where 100% refers to the initial state of the beam and 0 to the collapsed state. The estimates of the remaining capacity are defined by the ratio of the difference between the ultimate and applied load to the ultimate load. It can be observed that the decreasing trend of the natural frequency with reference to the decreasing remaining structural capacity is strikingly

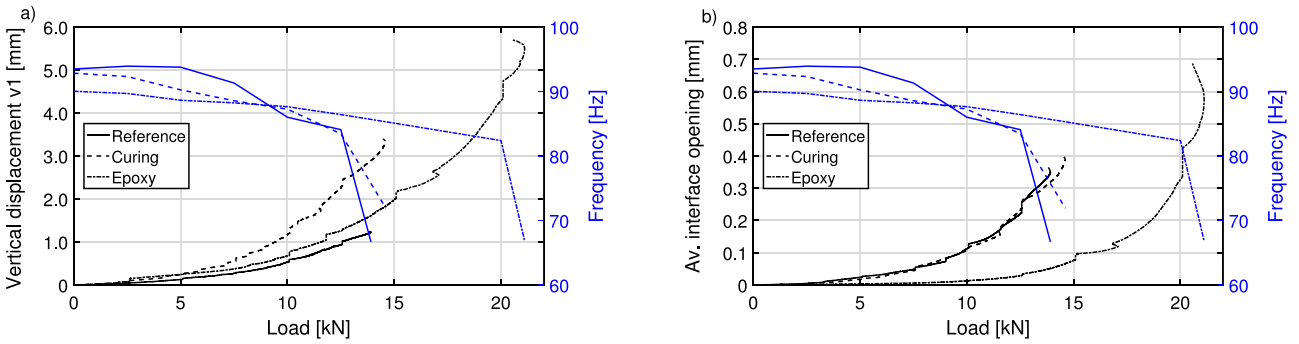

Fig. 17. (a) Vertical displacement and resonance frequency vs. applied load; (b) average joint opening between sensor v10 and v11 and resonance frequency vs. applied load.

similar among all the curves, irrespective of the type of beam. The similarity between these curves allows to draw some qualitative conclusions concerning the use of frequency variation for damage detection.

According to Fig. 18, and with respect to the Reference, Curing and Epoxy beam, a remaining structural capacity of 30% to 40% corresponds to a maximum decrease of the natural frequency of only 5%. Based on FE model 2.1, the Young's Modulus would need to be reduced by roughly 60% (see Fig. 15). A significant reduction in the resonant frequency (>5%) was observed only when the specimens were close to failure. At complete failure, the natural frequencies decreased by 20% to 30% for the different specimens. The final reduction is fairly in line with the identified variation of the first bending mode of damaged reinforced concrete beams available in the literature [47–54] (see also [55] for summary tables listing observed natural frequency variation). As shown in Fig. 18, the final natural frequency decrease is slightly higher than the 24% reduction reported in [51,52] for the first bending mode, and higher than 13% as reported in [53]. The most striking difference highlighted by Fig. 18 refers to the slope of variation of the normalized natural frequency vs. remaining structural capacity curves. The first bending mode of the three tested samples (Reference, Curing and Epoxy) seem to be quite insensitive to the induced damage, while the slope of all the other curves exhibit a higher steepness at earlier level of damage while reaching a plateau when approaching the ultimate load. The difference might be linked to the different damage mechanism the tested beam were subject to. The results summarized by the grey curves in Fig. 18 refer to natural frequency variations of reinforced concrete beams caused by the occurrence of flexural cracks finally resulting in the yielding of the reinforcement bars, while the damage and failure mechanism of the hybrid beams under investigation were driven by the interface behaviour (for the Reference and Curing sample) and by a predominant flexural cracking, combined with delamination, for the Epoxy sample. All the tested samples led to a brittle failure of the concrete at the end of the coupling reinforcement bar.

The low sensitivity of the natural frequency variation could be a significant limitation if a frequency-based damage detection approach would be used for early damage detection of hybrid structures. Note that the identified modes of vibration, during a typical ambient vibration monitoring campaign of civil infrastructures [2,43–46] usually include the first low-frequency global modes of the investigated structure. In this regard, there would be no need to further investigate the sensitivity of the higher bending modes of the tested beams as shown in [16–19], since it is highly unlikely that such modes would be excited by means of ambient vibration.

Despite the aforementioned limitation to detect delamination at an early phase, SHM approaches relying on frequency-shifts still comprise the majority of the implemented damage identification schemes for civil infrastructures, since it is a non invasive technique, it highlights the evolution in time of the global behaviour of a structure and it has the benefit of an intuitive physical interpretation due to the direct correlation between frequency and stiffness. In order to take full advantage of such SHM technique, an integrated approach linking laboratory activities, modelling studies, in situ monitoring campaigns and data science is needed. Such an integrated approach would allow to define limits and recommendations for a vibration-based monitoring strategy designed for detecting specific types of damage. With this in mind, the current study shows a possible direction in which laboratory activities and models are developed and assessed based on their capability of being used in a vibration-based SHM campaign of large-scale structures. To clarify, the simulated debonded layer and the corresponding Young's Modulus reduction shown in Section 4, could be used to predict the effect on natural frequencies of a simulated large-scale structure composed of hybrid structural elements prone to delamination issues (e.g. hybrid floor systems, strengthening applications, etc.). A sensitivity analysis on such large-scale model could be carried out by changing the extension of the delamination in order to pin down the natural frequencies exhibiting the highest sensitivity. Comparing the results from the sensitivity analysis with the typical observed variability of identified natural frequencies (mostly due to environmental effects, see [2,43–46]), may enable to estimate the minimum amount of damage that should be identified by adopting a frequency-based approach. As mentioned in the Introduction, damage detection strategies following the latter line of reasoning have been proposed often [13,22,24,25]. However, the chosen Youngs' Modulus reduction of specific regions in the FE model used to mimic a possible damage was arbitrarily selected without any direct link to actual measured damage patterns. The remaining drawback of this approach is that the resonance frequency which are usually identified during ambient vibration monitoring of civil structures are confined in the low frequency band (approximately below 30 Hz) and therefore less sensitive to local damages. Recent research efforts [57,58] focused on exploring new ways of monitoring interface-related damage by exploiting the use of piezoelectric sensors and measurements of the electromechanical impedance of the area surrounding a delamination. Alternatively to the frequency-based approach, a modal strain-based approach identified by means of Fibre Bragg Grating (FBG) sensor, as proposed in [59], seems also to be more sensitive to the occurrence of damage. The feasibility of these methods for hybrid concrete beams prone to brittle failures needs still to be tested.

6. Summary and conclusions

A comparative analysis concerning the developed damage mechanism along the interface of three novel hybrid concrete beams was presented. The tested beams, labelled as Reference, Curing and Epoxy, differed in terms of curing method and interface surface preparation. The damage was induced by step-wisely loading the beam in a four bending test setup. Vertical displacements and deformations were monitored and tracked by means of linear variable differential transformers (LVDTs) and the Digital Image Correlation (DIC) technique. The results of the load–displacement curves showed that the bending stiffness of the Curing sample is lower compared to the Reference sample, whereas the slope of the load–displacement curves between the Epoxy

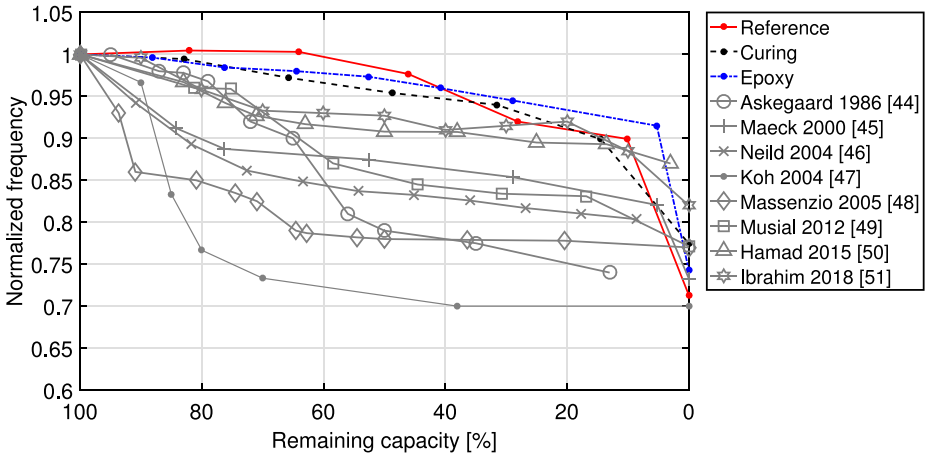

Fig. 18. Decrease of normalized frequency vs. remaining structural capacity, computed as a ratio between applied load and ultimate load. The graph compares the modal test results obtained in this paper with published results in [47–54,56].

and Reference samples almost overlap, indicating a similar bending stiffness. Although, the Curing sample was more prone to delamination compared to the Reference sample, at the same load levels, the different curing conditions did not affect the structural capacity between the Reference and Curing beam. Overall, the Epoxy sample exhibited a higher interface strength, exhibiting a significant difference in terms of fracture mechanism and structural capacity compared to the other two samples. The induced damage in the Reference and Curing samples was clearly triggered and driven by a delamination process along the interface, while in the Epoxy sample the damage initially developed as a vertical flexural crack up to a load of 10 kN, and kept developing further flexural cracks, combined with limited and localized delamination, until the brittle failure of the concrete occurred at the end of the coupling reinforcement bars. Although the capacity of the Epoxy sample was twice as large as that of the Reference and Curing, in none of the beams yielding of the coupling reinforcement was reached.

With regard to the dynamic test results, it can be concluded that the first natural frequencies of the tested beams were decreasing with progressive damage. However, significant reduction in the natural frequency was observed only when the specimens were close to the ultimate failure point. The natural frequency reduction of merely 5% for the first bending mode is observed at the load levels which were between 30% and 40% lower than the failure load. Similarly, the natural frequency reduction of 10% corresponded to the load level only 15% lower than the failure load. This indicates that frequency-based SHM, may not be sensitive enough to detect delamination for early-stage damage detection purposes of hybrid concrete structures. Interesting to notice was that when plotted as natural frequency versus structural capacity, all the beams showed almost the same behaviour. The final natural frequency reduction at failure is in line with the experimental observations for reinforced concrete beams from the literature, although the shape of the curves seems to be different. The difference might be related to a different type of failure observed in tested hybrid structures compared to regular reinforced concrete beams and slabs.

To conclude, further research efforts are necessary in order to develop a robust and sensitive vibration-based delamination detection technique and reliable models, suitable for monitoring large-scale structures composed of hybrid structural elements.

CRediT authorship contribution statement

Alessandro Cabboi: Conceptualization, Methodology, Software, Formal analysis, Writing – original draft, Writing – review & editing, Visualization. **Othman Harrass:** Data curation, Formal analysis, Investigation. **Sergio Sánchez Gómez:** Software. **Mladena Luković:** Conceptualization, Methodology, Formal analysis, Writing – original draft, Writing – review & editing, Visualization, Supervision, Funding acquisition.

Declaration of competing interest

The authors declare that they have no known competing financial interests or personal relationships that could have appeared to influence the work reported in this paper.

Acknowledgements

This work was supported by the Dutch Organization for Scientific Research (NWO), Netherlands under the grant “Optimization of interface behaviour for innovative hybrid concrete structures” (project number 16814). The authors would also like to thank Ir. J.M. Hendriks, from the Railway Engineering section at TU Delft, for lending us the data acquisition system and the instrumented hammer used for the dynamic tests.

References

[1] Brownjohn JMW. Structural health monitoring of civil infrastructure. Phil Trans R Soc A 2007;365(1851):589–622.
[2] Brownjohn JMW, De Stefano A, Xu Y-L, Wenzel H, Aktan AE. Vibration-based monitoring of civil infrastructure: challenges and successes. J Civ Struct Health Monit 2011;1(3):79–95.
[3] An Y, Chatzi E, Sim S-H, Laflamme S, Blachowski B, Ou J. Recent progress and future trends on damage identification methods for bridge structures. Struct Control Health Monit 2019;26(10):e2416.
[4] Pendhari SS, Kant T, Desai YM. Application of polymer composites in civil construction: A general review. Compos Struct 2008;84(2):114–24.
[5] Gibson RF. A review of recent research on mechanics of multifunctional composite materials and structures. Compos Struct 2010;92(12):2793–810.
[6] Muc A, Stawiarski A, Chwał M. Design of the hybrid FRP/concrete structures for bridge constructions. Compos Struct 2020;247:112490.
[7] Xu Y, Zhang H, Schlangen E, Luković M, Šavija B. Cementitious cellular composites with auxetic behavior. Cem Concr Compos 2020;111:103624.
[8] Zou X, Lin H, Feng P, Bao Y, Wang J. A review on FRP-concrete hybrid sections for bridge applications. Compos Struct 2021;262:113336.
[9] Ben S, Zhao J, Zhang Y, Qin Y, Rabczuk T. The interface strength and debonding for composite structures: Review and recent developments. Compos Struct 2015;129:8–26.
[10] Peng S, Wei Y. On the influence of interfacial properties to the bending rigidity of layered structures. J Mech Phys Solids 2016;92:278–96.
[11] Luković M, Hordijk D, Huang Z, Schlangen E. Strain hardening cementitious composite (SHCC) for crack width control in reinforced concrete beams. Heron 2019;64(1–2):189–206.
[12] Mustafa S, Singh S, Hordijk D, Schlangen E, Luković M. Experimental and numerical investigation on the role of interface for crack-width control of hybrid SHCC concrete beams. Eng Struct 2022;251:113378.
[13] Cabboi A, Gentile C, Saisi A. From continuous vibration monitoring to FEM-based damage assessment: Application on a stone-masonry tower. Constr Build Mater 2017;156:252–65.
[14] Borlenghi P, Gentile C, Saisi A. Detecting and localizing anomalies on masonry towers from low-cost vibration monitoring. Smart Struct Syst 2021;27(2):319–33.

[15] Zou Y, Tong L, Steven GP. Vibration-based model-dependent damage (delamination) identification and health monitoring for composite structures—a review. J Sound Vib 2000;230(2):357–78.

[16] Zhang Z, Shankar K, Morozov EV, Tahtali M. Vibration-based delamination detection in composite beams through frequency changes. J Vib Control 2016;22(2):496–512.

[17] Zhang Z, He M, Liu A, Singh HK, Ramakrishnan KR, Hui D, Shankar K, Morozov EV. Vibration-based assessment of delaminations in FRP composite plates. Composites B 2018;144:254–66.

[18] Sha G, Cao M, Radzieński M, Ostachowicz W. Delamination-induced relative natural frequency change curve and its use for delamination localization in laminated composite beams. Compos Struct 2019;230:111501.

[19] Sha G, Radzieński M, Cao M, Ostachowicz W. A novel method for single and multiple damage detection in beams using relative natural frequency changes. Mech Syst Signal Process 2019;132:335–52.

[20] Niemann H, Morlier J, Shahdin A, Gourinat Y. Damage localization using experimental modal parameters and topology optimization. Mech Syst Signal Process 2010;24(3):636–52.

[21] Khan A, Ko D-K, Lim SC, Kim HS. Structural vibration-based classification and prediction of delamination in smart composite laminates using deep learning neural network. Composites B 2019;161:586–94.

[22] Oliveira G, Magalhães F, Cunha A, Caetano E. Vibration-based damage detection in a wind turbine using 1 year of data. Struct Control Health Monit 2018;25(11):e2238.

[23] Tatsis K, Chatzi E. A numerical benchmark for system identification under operational and environmental variability. In: 8th IOMAC - International operational modal analysis conference. 2019, p. 101–6.

[24] García-Macías E, Ierimonti L, Venanzi I, Ubertini F. An innovative methodology for online surrogate-based model updating of historic buildings using monitoring data. Int J Archit Herit 2021;15(1):92–112.

[25] Pereira S, Magalhães F, Gomes JP, Cunha A, Lemos JV. Vibration-based damage detection of a concrete arch dam. Eng Struct 2021;235:112032.

[26] Girardi M, Padovani C, Pellegrini D, Robol L. A finite element model updating method based on global optimization. Mech Syst Signal Process 2021;152:107372.

[27] Momayez A, Ehsani M, Ramezanianpour A, Rajaie H. Comparison of methods for evaluating bond strength between concrete substrate and repair materials. Cem Concr Res 2005;35(4):748–57.

[28] Zanotti C, Randl N. Are concrete-concrete bond tests comparable? Cem Concr Compos 2019;99:80–8.

[29] Luković M, Schlangen H, Ye G, Savija B. Impact of surface roughness on the debonding mechanism in concrete repairs. In: FraMCoS-8: Proceedings of the 8th international conference on fracture mechanics of concrete and concrete structures, Toledo, Spain, 10-14 March, 2013. 2013.

[30] Wijte S. Onderzoek constructieve veiligheid breedplaatvloeren in bestaande utiliteitsgebouwe. Tech. Rep., Dossier 9780, Rapport 9780-1-0, Hageman B.V.; 2019.

[31] Lundgren K, Helgesson J, Sylvén R. Joints in lattice girder structures. Tech. Rep., Chalmers University of Technology; 2005.

[32] Jian Z. Performance of engineered cementitious composites for concrete repairs (Ph.D. thesis), TU Delft; 2011, URL: http://resolver.tudelft.nl/uuid:4bc07d00-4455-4c38-b97e-5a06e77d9ce7.

[33] 1992-1-1 EEN 1992-1-1 Eurocode 2. Eurocode 2 - Design of concrete structures - Part 1-1: General rules and rules for buildings, Vol. 1. 2011.

[34] Ewins DJ. Modal testing: Theory, practice, and application. 2nd ed., Baldock, Hertfordshire, England; 2000.

[35] Juang JN, Pappa RS. An eigensystem realization algorithm for modal parameter identification and model reduction. J Guid Control Dyn 1985;8(5):620–7.

[36] Jones E. Documentation for Matlab-based DIC code. University or Illinois; 2013.

[37] Luković M, Dong H, Šavija B, Schlangen E, Ye G, van Breugel K. Tailoring strain-hardening cementitious composite repair systems through numerical experimentation. Cem Concr Compos 2014;53:200–13.

[38] Smith M. ABAQUS/standard user's manual, version 6.14. United States: Dassault Systèmes Simulia Corp; 2014.

[39] Shih M-H, Sung W-P. Application of digital image correlation method for analysing crack variation of reinforced concrete beams. Sadhana 2013;38(4):723–41.

[40] Ghorbani R, Matta F, Sutton M. Full-field deformation measurement and crack mapping on confined masonry walls using digital image correlation. Exp Mech 2015;55:227–43.

[41] Luković M. Influence of interface and strain hardening cementitious composite (SHCC) properties on the performance of concrete repairs (Ph.D. thesis), TU Delft; 2016, URL: https://doi.org/10.4233/uuid:28b07d9b-c704-47fa-9ba3-cd9fde10130a.

[42] Šavija B, Schlangen E. On the use of a lattice model for analyzing of in-plane vibration of thin plates. Comput Mater Contin 2015;48(3):181–202.

[43] Rohrmann RG, Bässler M, Said S, Schmid W, Rücker W. Structural causes of temperature affected modal data of civil structures obtained by long time monitoring. In: 18th international modal analysis conference, San Antonio TX. 2000.

[44] Sohn H, Dzwonczyk M, Straser EG, Kiremidjian AS, Law KH, Meng T. An experimental study of temperature effect on modal parameters of the Alamosa Canyon Bridge. Earthq Eng Struct Dyn 1999;28(8):879–97.

[45] Olaf H, Glauco F, Johan M, Nedim K, Masoud M. Damage identification using modal data: Experiences on a prestressed concrete bridge. J Struct Eng 2005;131(12):1898–910.

[46] Peeters B, De Roeck G. One-year monitoring of the Z24-Bridge: environmental effects versus damage events. Earthq Eng Struct Dyn 2001;30(2):149–71.

[47] Askegaard V, Langœ HE. Correlation between changes in dynamic properties and remaining carrying capacity. Mater Struct 1986;19(1):11–9.

[48] Maeck J, Abdel Wahab M, Peeters B, De Roeck G, De Visscher J, De Wilde W, Ndambi J-M, Vantomme J. Damage identification in reinforced concrete structures by dynamic stiffness determination. Eng Struct 2000;22(10):1339–49.

[49] Neild SA, Williams MS, McFadden PD. Nonlinear vibration characteristics of damaged concrete beams. J Struct Eng 2003;129(2):260–8.

[50] Koh SJ, Maalej M, Quek ST. Damage quantification of flexurally loaded RC slab using frequency response data. Struct Health Monit 2004;3(4):293–311.

[51] Massenzio M, Jacquelin E, Ovigne PA. Natural frequency evaluation of a cracked RC beam with or without composite strengthening for a damage assessment. Mater Struct 2005;38(10):865–73.

[52] Musiał M. Static and dynamic stiffness of reinforced concrete beams. Arch Civ Mech Eng 2012;12(2):186–91.

[53] Hamad WI, Owen JS, Hussein MFM. Modelling the degradation of vibration characteristics of reinforced concrete beams due to flexural damage. Struct Control Health Monit 2015;22(6):939–67.

[54] Ibrahim Z, Hanif MU, Xin Lim H, Xian Hang Y. Effect of incremental static damage on modal frequencies of reinforced concrete beams. Int J Integr Eng 2018;10(2).

[55] Benedetti A, Pignagnoli G, Tarozzi M. Damage identification of cracked reinforced concrete beams through frequency shift. Mater Struct 2018;51(147).

[56] Pešić N, Živanović S, Dennis J, Hargreaves J. Experimental and finite element dynamic analysis of incrementally loaded reinforced concrete structures. Eng Struct 2015;103:15–27.

[57] Roth W, Giurgiutiu V. Structural health monitoring of an adhesive disbond through electromechanical impedance spectroscopy. Int J Adhes Adhes 2017;73:109–17.

[58] Tenreiro AFG, Lopes AM, da Silva LF. A review of structural health monitoring of bonded structures using electromechanical impedance spectroscopy. Struct Health Monit 2021. URL: https://doi.org/10.1177/1475921721993419; (in press).

[59] Anastasopoulos D, De Roeck G, Reynders EP. Influence of damage versus temperature on modal strains and neutral axis positions of beam-like structures. Mech Syst Signal Process 2019;134:106311.